RNA underediting, epileptic death of mutant mouse lines caused solely by a modest decrease (20 to 40%) in the editing efficiency of a single site (GluR-B Q/R site) has been reported (*26*). Our current efforts are focused on identification of the ADAR1 target genes critical for development.

References and Notes

1. B. L. Bass *et al.*, *RNA* **3**, 947 (1997).
2. S. M. Rueter, T. R. Dawson, R. B. Emeson, *Nature* **399**, 75 (1999).
3. M. Higuchi *et al.*, *Cell* **75**, 1361 (1993).
4. H. Lomeli *et al.*, *Science* **266**, 1709 (1994).
5. C. M. Burns *et al.*, *Nature* **387**, 303 (1997).
6. A. G. Polson, B. L. Bass, J. L. Casey, *Nature* **380**, 454 (1996).
7. T. Melcher *et al.*, *Nature* **379**, 460 (1996).
8. F. Lai, C.-X. Chen, K. C. Carter, K. Nishikura, *Mol. Cell. Biol.* **17**, 2413 (1997).
9. A. Gerber, M. A. O'Connell, W. Keller, *RNA* **3**, 453 (1997).
10. C.-X. Chen *et al.*, *RNA* **6**, 755 (2000).
11. G. A. Dabiri, F. Lai, R. A. Drakas, K. Nishikura, *EMBO J.* **15**, 34 (1996).
12. Q. Wang *et al.*, *J. Neurochem.* **74**, 1290 (2000).
13. U. Kim *et al.*, *Proc. Natl. Acad. Sci. U.S.A.* **91**, 11457 (1994).
14. T. Melcher *et al.*, *J. Biol. Chem.* **271**, 31795 (1996).
15. M. S. Paul, B. L. Bass, *EMBO J.* **17**, 1120 (1998).
16. Y. Wang, Y. Zeng, J. M. Murray, Nishikura, *J. Mol. Biol.* **254**, 184 (1995).
17. A. Nagy *et al.*, *Proc. Natl. Acad. Sci. U.S.A.* **90**, 8424 (1993).
18. Supplementary material is available at *Science* Online at www.sciencemag.org/cgi/content/full/290/5497/1765/DC1.
19. The functional ADAR1 mRNA levels were determined with 0.5 μg of total RNA extracted from ES cells or whole embryos with LightCycler-RNA Amplification Kit and LightCycler (Roche Molecular Biochemicals, Indianapolis, IN). To control for variations in sample preparation and RNA concentration measurement, all reverse transcriptase–polymerase chain reaction (RT-PCR) reactions were normalized for hypoxanthine phosphoribosyltransferase (HPRT) expression as described [P. Gadue *et al.*, *J. Exp. Med.* **190**, 1189 (1999)]. The following primers were used for detection of ADAR1 mRNA levels: MADAR1 sense, CCTGTGGAGTCCAGTGAT; and MADAR1 antisense, TGACAATAAAGGGATAGCGT. Because the region amplified corresponds to E12 and E13, which were deleted during targeting, the ADAR1 mRNA detected must be derived from the nontargeted ADAR1$^+$ allele.
20. A. Herb, M. Higuchi, R. Sprengel, P. H. Seeburg, *Proc. Natl. Acad. Sci. U.S.A.* **93**, 1875 (1996).
21. M. Higuchi *et al.*, *Nature* **406**, 78 (2000).
22. N. Ferrara *et al.*, *Nature* **380**, 439 (1996).
23. E. S. Russell, *Adv. Genet.* **20**, 357 (1979).
24. N. Hu, M. L. Gulley, J. T. Kung, E. Y.-H. P. Lee, *Cancer Res.* **57**, 4123 (1997).
25. M. L. Mucenski *et al.*, *Cell* **65**, 677 (1991).
26. D. Feldmeyer *et al.*, *Nature Neurosci.* **2**, 57 (1999).
27. A. L. Joyner, Ed., *Gene Targeting—a Practical Approach* (IRL, Oxford Univ. Press, Oxford, 1993).
28. F. Lai, C.-X. Chen, V. M.-Y. Lee, K. Nishikura, *J. Neurochem.* **69**, 43 (1997).
29. O. Railskin, D.-S. C. Cho, J. Sperling, K. Nishikura, R. Sperling, unpublished results.
30. J. B. Patterson, C. E. Samuel, *Mol. Cell. Biol.* **15**, 5376 (1995).

31. We thank A. Nagy for R1 cells; J. Wheeler, J. Golden, H. S. Baldwin, and K. Zarett for examination of histology sections and D. Solter and J. M. Murray for reading and comments on this manuscript. This work was supported by grants from NIH, the Human Frontier Program Organization, and the Doris Duke Charitable Foundation.

3 August 2000; accepted 17 October 2000

REPORTS

Down-Regulation of the Macrophage Lineage Through Interaction with OX2 (CD200)

Robert M. Hoek,[1] Sigrid R. Ruuls,[1] Craig A. Murphy,[1] Gavin J. Wright,[2] Ruth Goddard,[2] Sandra M. Zurawski,[1] Bianca Blom,[1] Margit E. Homola,[1] Wolfgang J. Streit,[3] Marion H. Brown,[2] A. Neil Barclay,[2] Jonathon D. Sedgwick[1]*

OX2 (CD200) is a broadly expressed membrane glycoprotein, shown here to be important for regulation of the macrophage lineage. In mice lacking CD200, macrophage lineage cells, including brain microglia, exhibited an activated phenotype and were more numerous. Upon facial nerve transection, damaged CD200-deficient neurons elicited an accelerated microglial response. Lack of CD200 resulted in a more rapid onset of experimental autoimmune encephalomyelitis (EAE). Outside the brain, disruption of CD200-CD200 receptor interaction precipitated susceptibility to collagen-induced arthritis (CIA) in mice normally resistant to this disease. Thus, in diverse tissues OX2 delivers an inhibitory signal for the macrophage lineage.

OX2 (now CD200) (*1*) is expressed in diverse cell types and tissues, ranging from splenic B lymphocytes to central nervous system (CNS) neurons (*2*, *3*). It shares a two-immunoglobulin (Ig)-domain arrangement with molecules involved in T lymphocyte regulation (*4*), including CD2, 2B4, CD80, and CD86, and is genetically linked to the latter two (*5*). However, the broad expression pattern of CD200 and the finding that CD200-receptor (CD200R) expression is restricted to myeloid lineage cells (*6*, *7*) points instead to a role for CD200 in regulation of myeloid-derived cells.

To investigate CD200 function, we generated CD200 gene-targeted mice using C57BL/6 embryonic stem cells (*8–10*). Heterozygous (+/−) and homozygous (−/−) mice were grossly normal in appearance, bred normally, exhibited a normal life-span, and showed no obvious behavioral changes. Immunohistochemical (*11*) and flow cytometric (*12*) staining with a new monoclonal antibody to murine CD200 (mCD200, OX90) (*13*) showed expression on neurons in the CNS and on B cells, follicular dendritic cells (FDCs), and endothelium in splenic tissue in wild-type (+/+) mice, but not −/− mice (*2*, *3*) (Fig. 1). By contrast, splenic myeloid-lineage cells of +/+ mice (CD11b$^+$ macrophages and granulocytes) expressed no CD200 (Fig. 1). Levels of expression of B220, CD4, CD8, and CD11b were comparable between CD200−/− and +/+ mice (Fig. 1B). In the spleen of CD200$^{-/-}$ mice, changes were detected only in the CD11b$^+$ population, which doubled in size (Fig. 1B and Table 1), with both F4/80^{lo}-GR1^{hi} granulocytes and F4/80^{hi}-GR1^{lo} mature macrophages expanded significantly (Table 1). Thus, the absence of CD200 resulted in an increase in cells that do not express CD200, but rather its receptor (*7*).

The increased CD11b$^+$ population in CD200$^{-/-}$ mice was reflected in splenic red pulp enlargement, visualized by a larger surface area staining with F4/80 (Fig. 2, A and B). MOMA-1$^+$ metallophilic marginal zone macrophages were transformed from a thin, single cell layer (*14*) to a thick, multicell layer (Fig. 2, C and D). Higher expression of the ITAM-containing intracellular activation protein DAP12, shown to be an essential component of normal myeloid cell function (*15*), indicated that macrophage populations were activated in CD200$^{-/-}$ mice, particularly in the marginal zone (Fig. 2, E and F). Dendritic cells (DCs), which are CD200R$^+$ (*7*) and reside in the T cell area of the white pulp, also showed increased activation.

CD200$^{-/-}$ mice had slightly enlarged lymph nodes, especially the mesenteric lymph nodes (MLNs), changing from interconnected but well-defined spherical structures in +/+ mice (Fig. 2G) to a tubular formation, without clear demarcation between nodes (Fig. 2H). In addition, lymph node macrophages were expanded and activated substantially in CD200$^{-/-}$ mice (Fig. 2H).

Because microglia, the resident CNS macrophage (*16*, *17*), are CD200R$^+$ (*7*), neurons could in principle interact with and regulate microglia function through their expression of CD200 (Fig. 1A) (*3*). In healthy +/+ mice, microglia are quiescent cells expressing mole-

[1]DNAX Research Institute of Molecular and Cellular Biology, 901 California Avenue, Palo Alto, CA 94304, USA. [2]Sir William Dunn School of Pathology, University of Oxford, Oxford OX1 3RE, UK. [3]Department of Neuroscience, College of Medicine and Brain Institute, University of Florida, Gainsville, FL 32610, USA.

*To whom correspondence should be addressed. E-mail: jon.sedgwick@dnax.org

cules such as major histocompatibility complex class I and II, CD11b, and CD45 at low or negligible levels (Fig. 2, I and K) (*16*–*18*) and show an ordered, ramified appearance (Fig. 2I). In contrast, microglia of CD200$^{-/-}$ mice spontaneously exhibited many features of activation, including less ramified, shorter glial processes, a disordered arrangement (Fig. 2J), and increased CD11b and CD45 expression (Fig. 2, J and L). Unexpectedly, microglia in CD200$^{-/-}$ animals formed aggregates, strongly expressing CD11b and CD45, especially in the spinal cord (Fig. 2, J and L). Aggregation of microglia is seen rarely in normal healthy CNS, but is associated with inflammation or neurodegeneration (*18*).

To assess whether CD200 deficiency in the

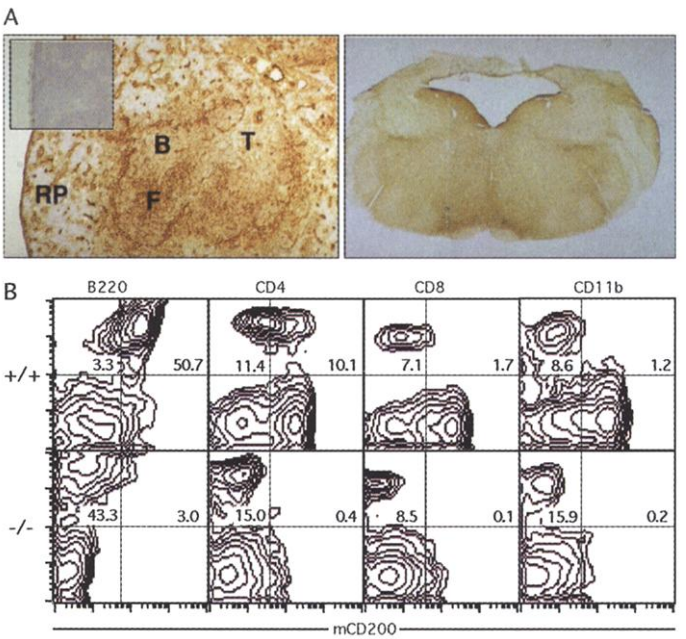

Fig. 1. (**A**) Immunohistochemical staining (*11*) for mCD200 of wild-type spleen (left) and brainstem (right). B, B cell follicles; T, T cell area; F, FDC; RP, red pulp. Staining is absent in CD200$^{-/-}$ mice (inset). (**B**) Flow cytometric analysis (*12*) of splenocytes. Numbers in quadrants are the percentages of total viable cells.

Table 1. Number of cells in splenocyte subpopulations in CD200$^{+/+}$ and −/− mice.

Phenotype	CD200$^{+/+}$*	CD200$^{-/-}$*
Total	43.8 ± 2.9	48.5 ± 2.5
B220^{+}	19.3 ± 1.8	21.4 ± 1.1
αβTCR^{+}	16.2 ± 1.3	13.1 ± 1.2
CD4^{+}	9.0 ± 0.9	7.3 ± 0.7
CD8^{+}	5.5 ± 0.6	4.5 ± 0.3
CD11b^{+}	4.1 ± 0.8	8.1 ± 0.6‡
F4/80^{hi}/GR1^{lo}†	1.8 ± 0.2	3.1 ± 0.2‡
GR1^{hi}/F4/80^{lo}†	1.6 ± 0.2	4.8 ± 0.6‡

*Mean number of cells ($\times 10^{-6}$) ± SEM, determined by multiplying the percentage of a given cell type (compare with Fig. 1B) with the viable cell count (n = 6). †By three-color flow cytometry CD11b^{+} cells were subdivided into macrophage (F4/80^{hi}/GR1^{lo}) and granulocyte (GR1^{hi}/F4/80^{lo}) populations. Note that the spleen contains more macrophages than granulocytes, but recovery of macrophages is suboptimal owing to interaction with splenic stromal elements and adherence properties. ‡Significantly higher number of cells in CD200$^{-/-}$ compared with +/+ mice ($P < 0.005$; unpaired t test).

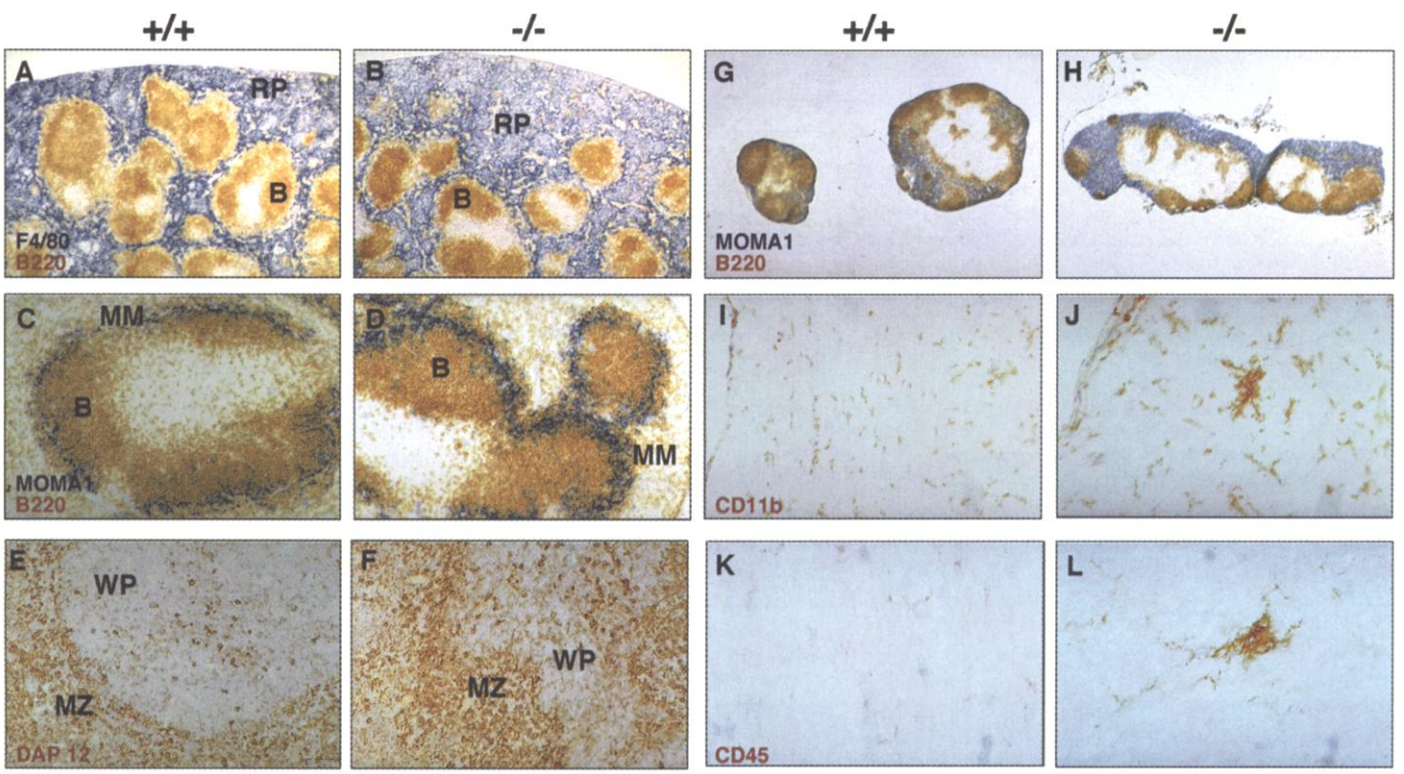

Fig. 2. CD200-deficient lymphoid tissues and CNS show dysregulated macrophage and myeloid compartments. Immunohistochemical analysis (*11*) of otherwise unmanipulated mice. [(A) to (F)] An expanded and more activated macrophage compartment in the spleen of CD200$^{-/-}$ mice. (**A** and **B**) Macrophages (F4/80, blue) and B lymphocytes (B220, brown); (**C** and **D**) metallophilic macrophages (MOMA-1, blue) and B lymphocytes (brown); MM, metallophilic macrophages; (**E** and **F**) DAP12 myeloid cell activation protein. WP, white pulp (collectively T and B lymphocyte areas); MZ, marginal zone. (**G** and **H**) Fused MLNs and more numerous lymph node macrophages (MOMA-1, blue) in CD200$^{-/-}$ mice. (**I** to **L**) Spontaneously activated and aggregated spinal cord microglia in mice lacking CD200 with up-regulated CD11b [(I) and (J)] and CD45 [(K) and (L)]. Histology is representative of analysis of 10 mice. Paired plates are at the same final magnification. Original magnifications: ×50 [(A) and (B)]; ×125 [(C) and (D)]; ×100 [(E) and (F)]; ×26 [(G) and (H)]; ×250 [(I) and (J)]; and ×500 [(K) and (L)].

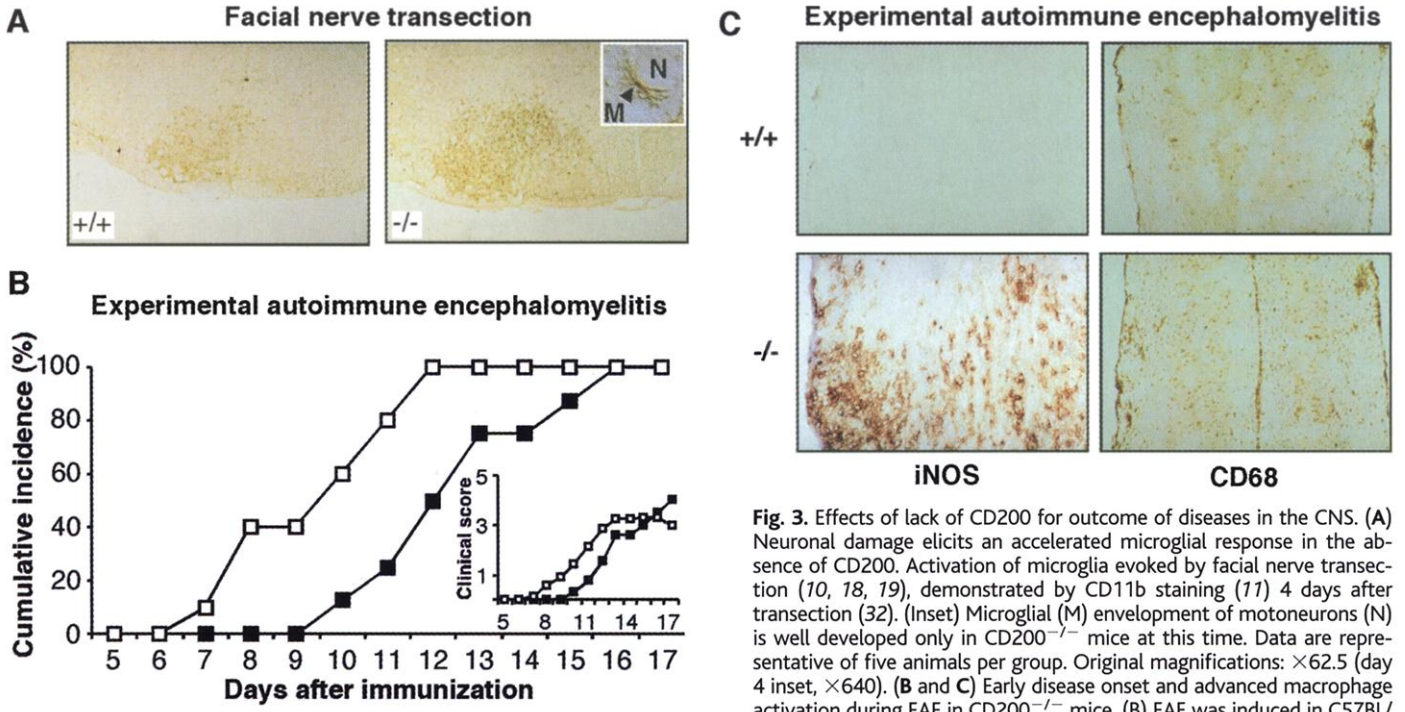

Fig. 3. Effects of lack of CD200 for outcome of diseases in the CNS. (**A**) Neuronal damage elicits an accelerated microglial response in the absence of CD200. Activation of microglia evoked by facial nerve transection (*10*, *18*, *19*), demonstrated by CD11b staining (*11*) 4 days after transection (*32*). (Inset) Microglial (M) envelopment of motoneurons (N) is well developed only in CD200$^{-/-}$ mice at this time. Data are representative of five animals per group. Original magnifications: ×62.5 (day 4 inset, ×640). (**B** and **C**) Early disease onset and advanced macrophage activation during EAE in CD200$^{-/-}$ mice. (B) EAE was induced in C57BL/6$^{+/+}$ (■) or CD200$^{-/-}$ (□) mice (*23*). Main graph shows the cumulative incidence; inset shows the mean of clinical scores at each time point (−/−: n = 10, +/+: n = 8). Mean day of onset ± SEM = 9.7 ± 0.6 (−/−) and 12.8 ± 0.7 (+/+); $P < 0.01$, unpaired t test. The data are representative of two separate experiments. Clinical scores ranged from tail weakness (score 1), through bilateral hind-limb paralysis and incontinence (score 5). (C) Immunohistochemistry of thoracic spinal cord (*11*) showed advanced macrophage activation in CD200$^{-/-}$ mice with disease at day 7 after immunization, shown by iNOS expression. At this stage the +/+ mice were healthy. Ten days after immunization, choosing a +/+ and −/− mouse that showed similar disease, macrophage and microglial activation across the entire tissue was still markedly enhanced in CD200$^{-/-}$ mice (CD68 staining). Original magnifications used: ×160 (iNOS); ×50 (CD68).

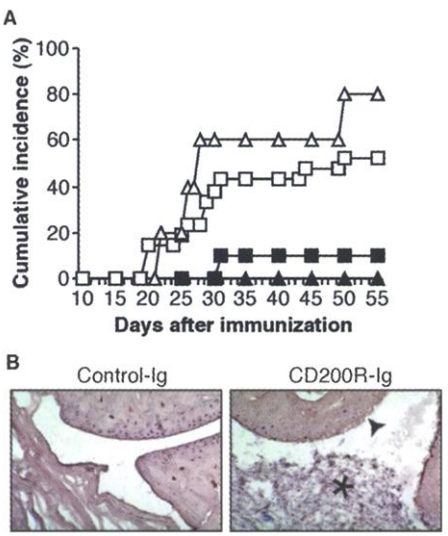

Fig. 4. Prevention of CD200-CD200R interaction renders C57BL/6 mice susceptible to CIA. (**A**) After a single immunization (*26*), a marked susceptibility increase to CIA is seen in CD200$^{-/-}$ mice (□) (n = 21) compared with +/+ (■) (n = 10) mice ($P < 0.025$, uncorrected χ^2 test), or when CD200-CD200R interaction is blocked in C57BL/6$^{+/+}$ mice with a soluble neutralizing CD200R-Ig fusion protein (*27*) (△) (n = 5), compared with control-Ig (Fc portion of human IgG only (▲) (n = 5) ($P < 0.01$, uncorrected χ^2 test). Incidence was determined by including mice with any clinical disease, scored on the appearance of swelling of a single joint (score 1), two or more joints (score 2), or the entire paw (score 3), summed over all four paws to give a maximum possible score of 12. A summary of the clinical data is shown in (*10*). (**B**) Histopathology of joints of a CD200R-Ig–treated mouse with disease and a he ithy control-Ig–treated animal at day 33. Hematoxylin and eosin staining show synovial inflammation (asterisk) and articular cartilage erosion (arrowhead) in the CD200R-Ig–treated, but not in the control-Ig–treated, animal. Micrographs shown are of metatarsophalangial joints. Original magnifications, ×125.

CNS affected microglial responsiveness to nerve damage, we used the facial nerve transection model for localized microglia activation (*19*). The course of microglial activation in +/+ mice is well documented (*19*) and can first be detected 4 days after transection (Fig. 3A), with the peak of activation at day 7 (*20*). In CD200$^{-/-}$ mice the microglial response was accelerated dramatically, with a detectable reaction after 2 days (*20*) and maximal activation 4 days after surgery (Fig. 3A). Microglial envelopment of damaged motoneurons (*18*, *19*) was well advanced in CD200$^{-/-}$ mice at day 4 (Fig. 3A, inset), but minimal at this time in +/+ mice.

To determine whether CD200 could limit disease processes to which myeloid lineage cells contribute, we used two autoimmune models affecting different tissues. The first, experimental autoimmune encephalomyelitis (EAE), is a model of the human disease multiple sclerosis, resulting from activation of peripheral T lymphocytes, macrophages (*21*), and granulocytes (*22*). These cells migrate to the CNS, leading to microglial activation, tissue damage, and neurological deficits including paralysis. Normal C57BL/6$^{+/+}$ mice are highly susceptible to EAE induced with MOG peptide (*23*), with onset occurring rapidly 10 days after immunization. Notably, MOG-induced EAE was advanced significantly by a further 3 days in the absence of CD200 (Fig. 3B). The presence of activated [inducible nitric oxide synthase (iNOS)–expresssing] inflammatory macrophages in the CNS of CD200$^{-/-}$ but not +/+ mice early in the disease confirmed these differences (Fig. 3C). Macrophage and microglia activation throughout the CNS, measured by CD68 expression, was greatly enhanced in CD200$^{-/-}$ mice compared with +/+ mice with disease (Fig. 3C). The relative contribution of the myeloid compartment in the CNS (microglia) (Figs. 2, I to L, and 3A) versus the periphery (macrophages) remains to be established.

CIA, a model of rheumatoid arthritis, is an inflammatory autoimmune disease of the joints, and like EAE involves tissue-specific influx of T cells, macrophages, and granulocytes. Macrophage products are critical elements of the disease process, leading ultimately to cartilage and bone destruction (*24*). In contrast to EAE, C57BL/6$^{+/+}$ mice are resistant to CIA after a

single immunization with collagen, with an extremely low incidence (<10%, Fig. 4A) (*25*). Immunizing CD200$^{-/-}$ mice only once (*26*) resulted in disease onset as early as day 20 and a cumulative incidence of over 50% (Fig. 4A). That this result was not an artifact of gene targeting was illustrated by infecting C57BL/6$^{+/+}$ mice with a replication-deficient adenovirus expressing a soluble Ig-fusion protein of CD200R (*7*, *27*). Such mice were highly susceptible to CIA compared with mice receiving a control Ig-fusion protein construct (Fig. 4A). Both CD200$^{-/-}$ and CD200R-Ig–treated animals developed moderate to severe arthritis (*10*) with synovial inflammation and formation of invasive pannus, resulting in cartilage and bone degradation seen normally only in CIA-susceptible animals (*24*) (Fig. 4B). Inflammatory cells in the arthritic joints were mainly CD11b^{+} cells (*20*), with a substantial proportion being CD68^{+} macrophages (*10*).

Because EAE and CIA are initiated by activation of self-reactive T lymphocytes (*21*, *25*), enhanced disease could reflect hyperactivation of these cells in the absence of CD200. No evidence for T cell dysregulation in CD200-deficient environments was observed with a range of in vivo and in vitro experiments (*10*).

Thus, through CD200 expression, diverse tissues regulate macrophages, and probably also granulocytes, directly and continuously through interaction with the inhibitory CD200R (*7*). The consequences of loss of this pathway can be profound, rendering mice susceptible to tissue-specific autoimmunity and enabling accelerated reactivity of resident tissue macrophages, including those in the CNS. That these effects appear to be unrelated to T cell activation but rather the result of direct deregulation of effector pathways within the macrophage/myeloid lineage has important and broad implications for treatment of neurodegenerative diseases like Alzheimer's disease or for varied pathologies involving hyperactivation of the myeloid lineage.

References and Notes

1. HLDA7: 7th Workshop and Conference on Human Leukocyte Differentiation Antigens, Harrogate, UK, 20 to 24 June 2000.
2. A. N. Barclay, *Immunology* **42**, 727 (1981).
3. M. Webb, A. N. Barclay, *J. Neurochem.* **43**, 1061 (1984).
4. S. J. Davis *et al.*, *Immunol. Rev.* **163**, 217 (1998).
5. F. Borriello *et al.*, *Mamm. Genome* **9**, 114 (1998).
6. S. Preston *et al.*, *Eur. J. Immunol.* **27**, 1911 (1997).
7. G. J. Wright *et al.*, *Immunity* **13**, 233 (2000).
8. F. A. Lemckert, J. D. Sedgwick, H. Körner, *Nucleic Acids Res.* **25**, 917 (1997).
9. F. Köntgen *et al.*, *Int. Immunol.* **5**, 957 (1993).
10. Supplementary data are available at *Science* Online at www.sciencemag.org/cgi/content/full/290/5497/1768/DC1.
11. Single- and double-staining procedures used are detailed in (*28*). Primary antibodies were as in (*12*), and MOMA-1 (Bachem Bioscience, King of Prussia, PA), rabbit polyclonal anti-DAP12 antibody (*15*), and anti-CD45 (clone YTS165.1 obtained from S. P. Cobbold, University of Oxford, UK). Secondary antibodies were peroxidase- or alkaline phosphatase–conjugated polyclonal anti-rat or anti-rabbit IgG (Jackson Immunochemicals, NJ). Hind limbs for histological analysis were prepared by means of a procedure adapted from (*29*).
12. Single-cell suspensions of spleens were stained for mCD200 (*13*), B220, CD4, CD8, CD11b, Ly-6G, and F4/80 (PharMingen, San Diego, CA, and Caltag, Burlingame, CA) by standard procedures.
13. OX90 was prepared by fusing splenocytes from rats immunized with a mouse CD200–rat CD4 fusion protein (*6*) with the Y3 myeloma, by standard procedures. The monoclonal antibody was selected by its capacity to bind recombinant mCD200–rat CD4 in an enzyme-linked immunosorbent assay (ELISA) and to bind those cells predicted to express CD200 (*2*, *3*).
14. G. Kraal, M. Janse, *Immunology* **58**, 665 (1986).
15. A. B. H. Bakker *et al.*, *Immunity* **13**, 345 (2000).
16. V. H. Perry, S. Gordon, *Trends Neurosci.* **11**, 273 (1988).
17. J. D. Sedgwick *et al.*, *Proc. Natl. Acad. Sci. U.S.A.* **88**, 7438 (1991).
18. G. W. Kreuzberg, *Glia* **19**, 312 (1996).
19. M. B. Graeber, W. J. Streit, G. W. Kreutzberg, *J. Neurosci. Res.* **21**, 18 (1988).
20. R. M. Hoek *et al.*, data not shown.
21. C. S. Raine, *Lab. Invest.* **50**, 608 (1984).
22. S. R. McColl, *et al.*, *J. Immunol.* **161**, 6421 (1998).
23. EAE was induced and scored as described in (*30*) by subcutaneous immunization with 50 μg of myelin oligodendrocyte glycoprotein $(MOG)_{35-55}$ peptide in complete Freund's adjuvant (CFA), but each mouse received 0.1 mg of H37RA *Mycobacterium tuberculosis* and intravenous injections of 100 ng of pertussis toxin on the day of immunization and 2 days later.
24. I. K. Campbell *et al.*, *Ann. Rheum. Dis.* **56**, 364 (1997).
25. W. C. Watson, A. S. Townes, *J. Exp. Med.* **162**, 1878 (1985).
26. CIA was induced by immunization intradermally with 100 μg of chicken type II collagen in CFA (0.25 mg H37RA *M. tuberculosis*) and scored only by clinical criteria as described in (*24*).
27. The adapted mCD200R cDNA (residues 86 to 720) was subcloned in the Xho I site of a modified pCDM8.Ig expression plasmid (*31*). The Hind III–Not I fragment of this was transferred to a modified pQB1-AdCMV5-GFP adenovirus transfer vector (Quantum Biotechnologies, Montreal, Canada), with an additional multicloning site 5′-AGATCTAAGCTTGCACGCGTATGCGGCCGCATGGTACCATTCTAGAGCGATATCGTTTAA AC-3′ added between the Bgl II and Pme I sites. Recombinant adenovirus was produced with host QBI-293A human embryonic kidney cells (Quantum applications manual 24AL98). Virus expressing only the human Fc portion encoded by pCDM8.Ig was used as control. Mice were infected 5 days before collagen immunization, and serum human Ig levels were subsequently monitored by ELISA.
28. J. D. Sedgwick *et al.*, *J. Exp. Med.* **177**, 1145 (1993).
29. R. Jonsson, A. Tarkowski, L. Klareskog, *J. Immunol. Methods* **88**, 109 (1986).
30. D. S. Riminton *et al.*, *J. Exp. Med.* **187**, 1517 (1998).
31. E. E. Bates *et al.*, *Mol. Immunol.* **35**, 513 (1998).
32. At various times after facial nerve transection (*19*), tissue was prepared for immunohistochemistry (*11*) of the brainstem area containing nucleus VII. To ensure valid comparison between different tissues, we made 20-μm coronal sections in a caudo-rostral direction starting in the cervical spinal cord, and advancing until the first appearance of nucleus VII. Eight-micrometer serial sections were prepared, and microglial activation was assessed (*11*, *19*).

33. We thank F. A. Lemckert and D. S. Riminton (Centenary Institute, Sydney, Australia) for technical assistance, N. Hutchings (University of Oxford, UK) for analysis of OX90 mAb, and L. Spargo (Hanson Centre, Adelaide, Australia) for advice on preparation of CIA tissue. We thank L. L. Lanier (UCSF, CA) and A. B. H. Bakker (DNAX, CA) for DAP12 antiserum, S. Gordon (University of Oxford, UK) for CD68 mAb, Y.-J. Liu (DNAX, CA) for support with DC studies, and M. Andonion for graphics assistance. Co-workers in Oxford were supported by the UK Medical Research Council. DNAX Research Institute is supported by Schering Plough Corporation.

14 August 2000; accepted 27 October 2000

Accumulation of Dietary Cholesterol in Sitosterolemia Caused by Mutations in Adjacent ABC Transporters

Knut E. Berge,[1]* Hui Tian,[3]* Gregory A. Graf,[1] Liqing Yu,[1] Nick V. Grishin,[2] Joshua Schultz,[3] Peter Kwiterovich,[4] Bei Shan,[3] Robert Barnes,[1] Helen H. Hobbs[1]†

In healthy individuals, acute changes in cholesterol intake produce modest changes in plasma cholesterol levels. A striking exception occurs in sitosterolemia, an autosomal recessive disorder characterized by increased intestinal absorption and decreased biliary excretion of dietary sterols, hypercholesterolemia, and premature coronary atherosclerosis. We identified seven different mutations in two adjacent, oppositely oriented genes that encode new members of the adenosine triphosphate (ATP)–binding cassette (ABC) transporter family (six mutations in *ABCG8* and one in *ABCG5*) in nine patients with sitosterolemia. The two genes are expressed at highest levels in liver and intestine and, in mice, cholesterol feeding up-regulates expressions of both genes. These data suggest that ABCG5 and ABCG8 normally cooperate to limit intestinal absorption and to promote biliary excretion of sterols, and that mutated forms of these transporters predispose to sterol accumulation and atherosclerosis.

In humans, the intestine presents a barrier that prevents the absorption of plant sterols and partially blocks the absorption of cholesterol. This barrier is disrupted in the rare autosomal recessive disorder, sitosterolemia, which is characterized by hyperabsorption of plant ste-